Figures

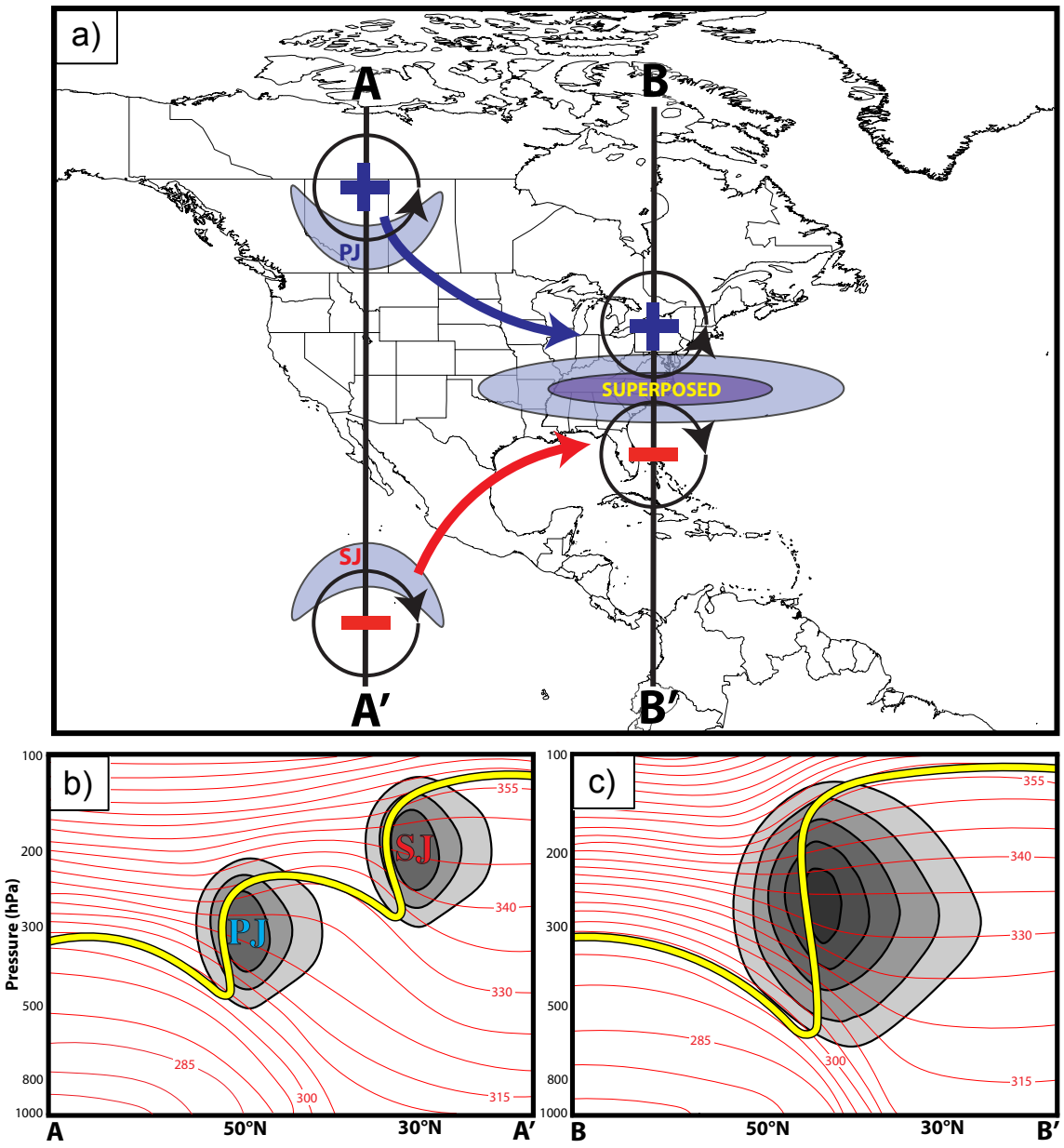

FIG. 1. (a) Conceptual model summarizing the development of a jet superposition. The plus sign and the minus sign correspond to a polar cyclonic and tropical anticyclonic PV anomaly, respectively, with the blue and red arrows indicating the movement of each PV anomaly towards middle latitudes. The purple fill corresponds to isotachs, with the darker shade of purple identifying stronger wind speeds. (b) Idealized cross section along A–A', as indicated in (a), through a separate polar jet (PJ) and subtropical jet (SJ). Wind speed (gray shading with darker shades of gray identifying stronger wind speeds), potential temperature (red lines every 5 K), and the 2-PVU contour (thick yellow line). (c) As in (b), but for the idealized cross section B–B', as indicated in (a), through a jet superposition. Figure and caption are adapted from Winters et al. (2020; their Fig. 1).

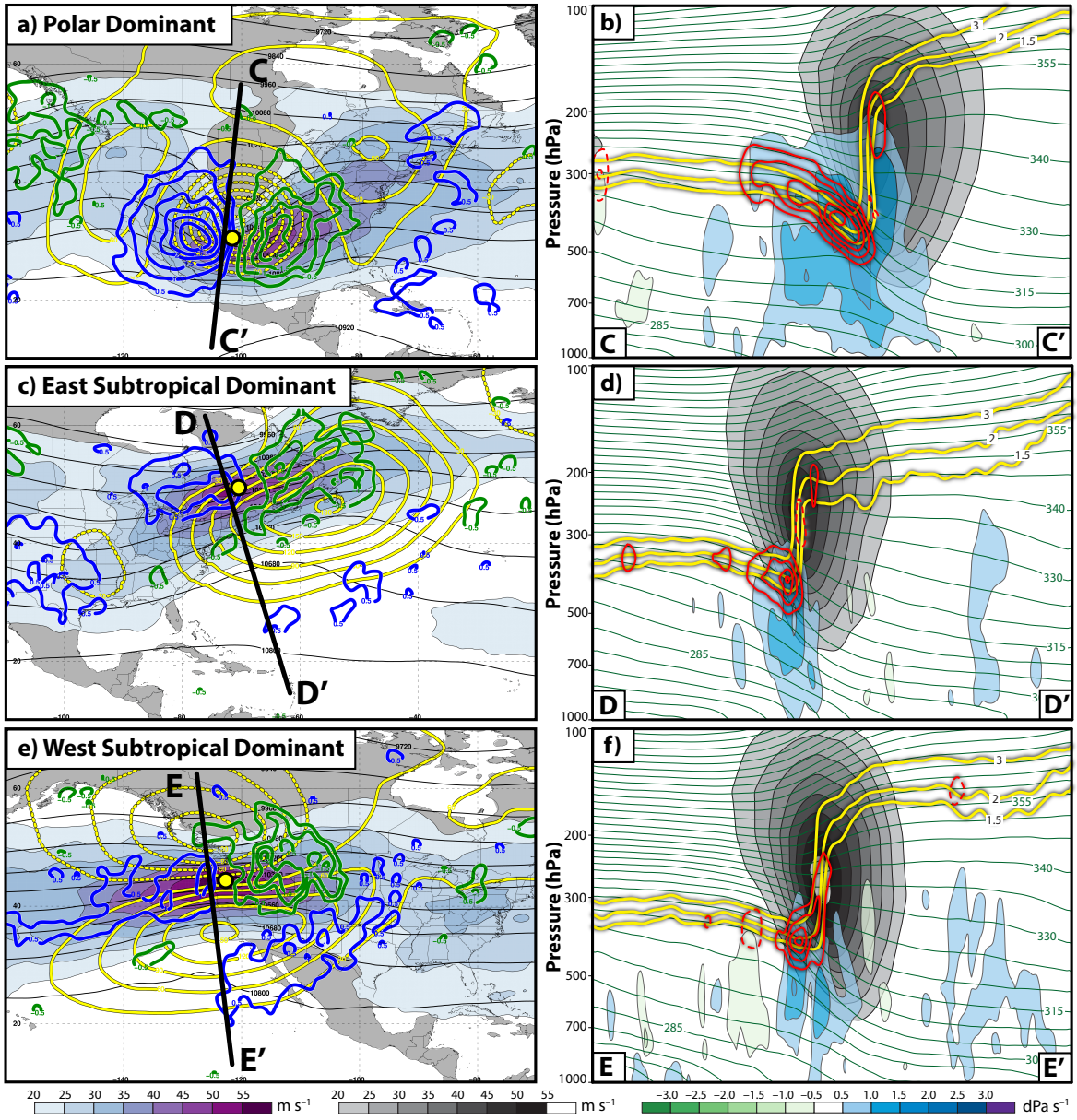

FIG. 2. (left) Composite 250-hPa geopotential height (black solid lines every 120 m), 250-hPa geopotential height anomalies (yellow lines every 30 m, solid when positive and dashed when negative), 250-hPa wind speed (shaded according to the legend in m s^{-1}), and 500-hPa vertical motion (contoured every 0.5 dPa s^{-1} in green for ascent and blue for descent) at the time of superposition for (a) polar dominant, (c) eastern subtropical dominant, and (e) western subtropical dominant jet superposition events. (right) Composite potential temperature (green lines every 5 K), wind speed (gray shading according to the legend in m s^{-1}), the 1.5-, 2-, and 3-PVU contours (yellow lines), PV advection by the three-dimensional divergent circulation (red lines every 0.5 × 10^{-5} PVU s^{-1}, solid when positive and dashed when negative), and vertical motion (shaded according to the legend in dPa s^{-1}) for (b) the cross section along C–C', as indicated in (a), (d) the cross section along D–D', as indicated in (c), and (f) the cross section along E–E', as indicated in (e). Figure and caption are adapted from Winters et al. (2020; their Figs. 5, 7b, 8, 10b, 11, 13b).

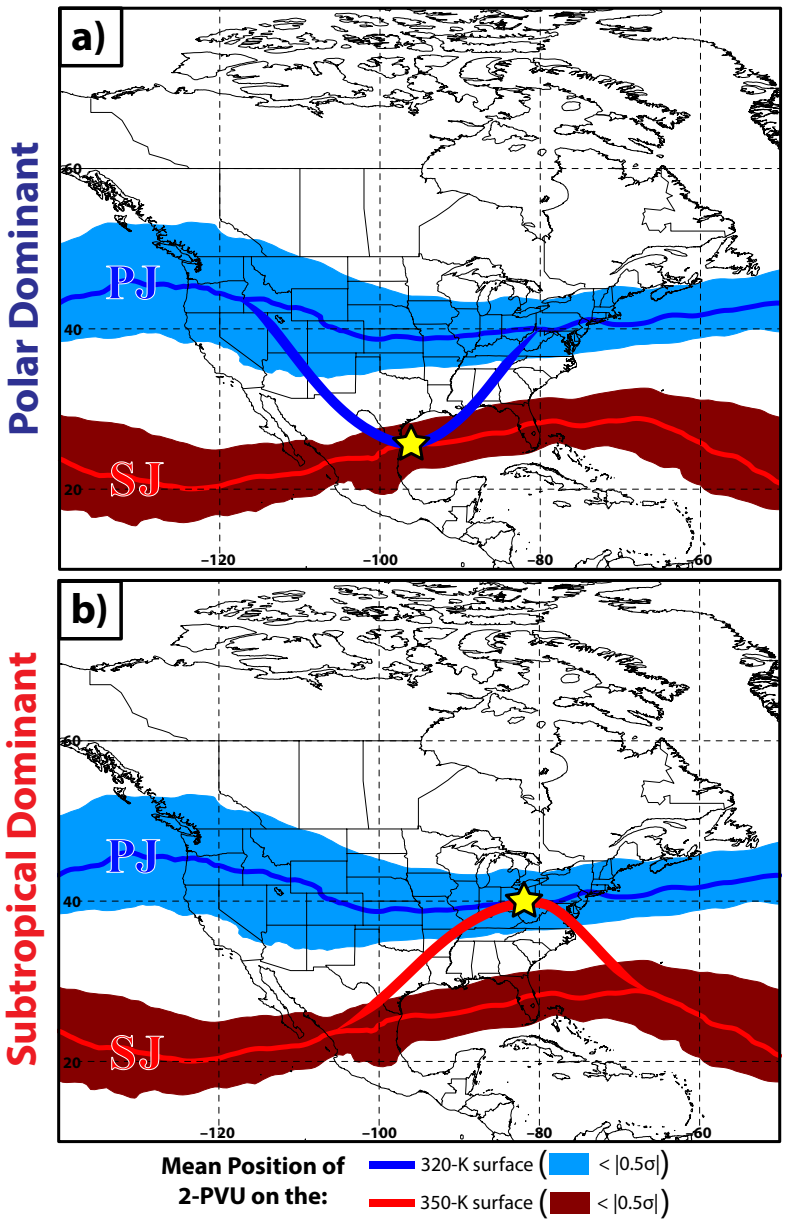

FIG. 3. The mean position of the 2-PVU contour on the 320-K and 350-K surfaces at 0000 UTC 1 January is indicated by the thin blue line and thin red line, respectively, as a proxy for the position of the polar jet (PJ) and subtropical jet (SJ) waveguide. Shaded areas bounding each mean 2-PVU contour indicate locations at which an observation of 2-PVU on that particular isentropic surface would represent a standardized PV anomaly with a magnitude less than 0.5. A hypothetical deviation of the 2-PVU contour from its mean position on the 320-K surface during the formation of a (a) polar dominant jet superposition event (yellow star) is indicated by the thick blue contour. (b) As in (a), but for a subtropical dominant event. A hypothetical deviation of the 2-PVU contour from its mean position on the 350-K surface during the formation of a subtropical dominant event is indicated by the thick red contour. Figure and caption adapted from Winters et al. (2020; their Fig. 2).

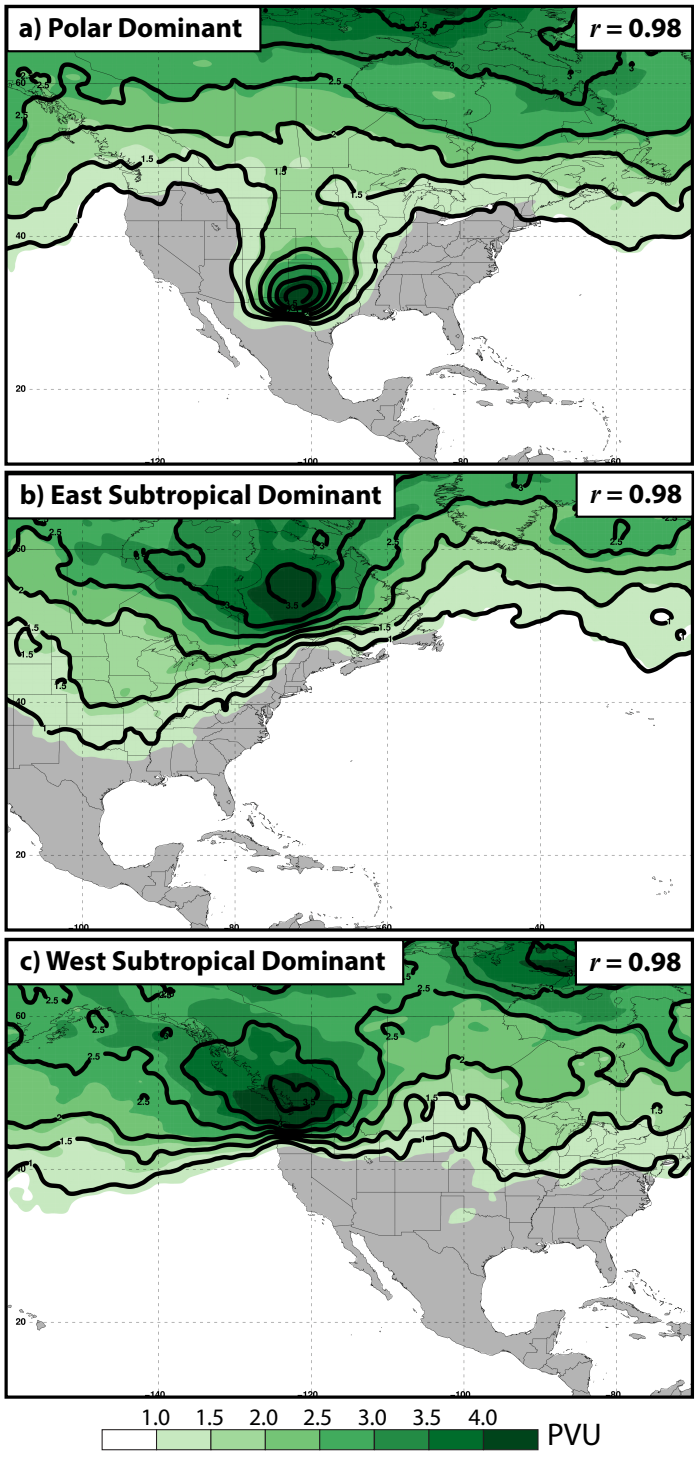

FIG. 4. 300-hPa Ertel PV (green shading according to the legend in PVU) and 300-hPa QGPV (scaled by $-g(\partial\Theta_r/\partial p)$; black lines every 0.5 PVU above 1 PVU) for (a) polar dominant, (b) eastern subtropical dominant, and (c) western subtropical dominant events at the time of jet superposition. The value in the top right of each panel indicates the spatial correlation between the 300-hPa Ertel PV and 300-hPa QGPV for each event type.

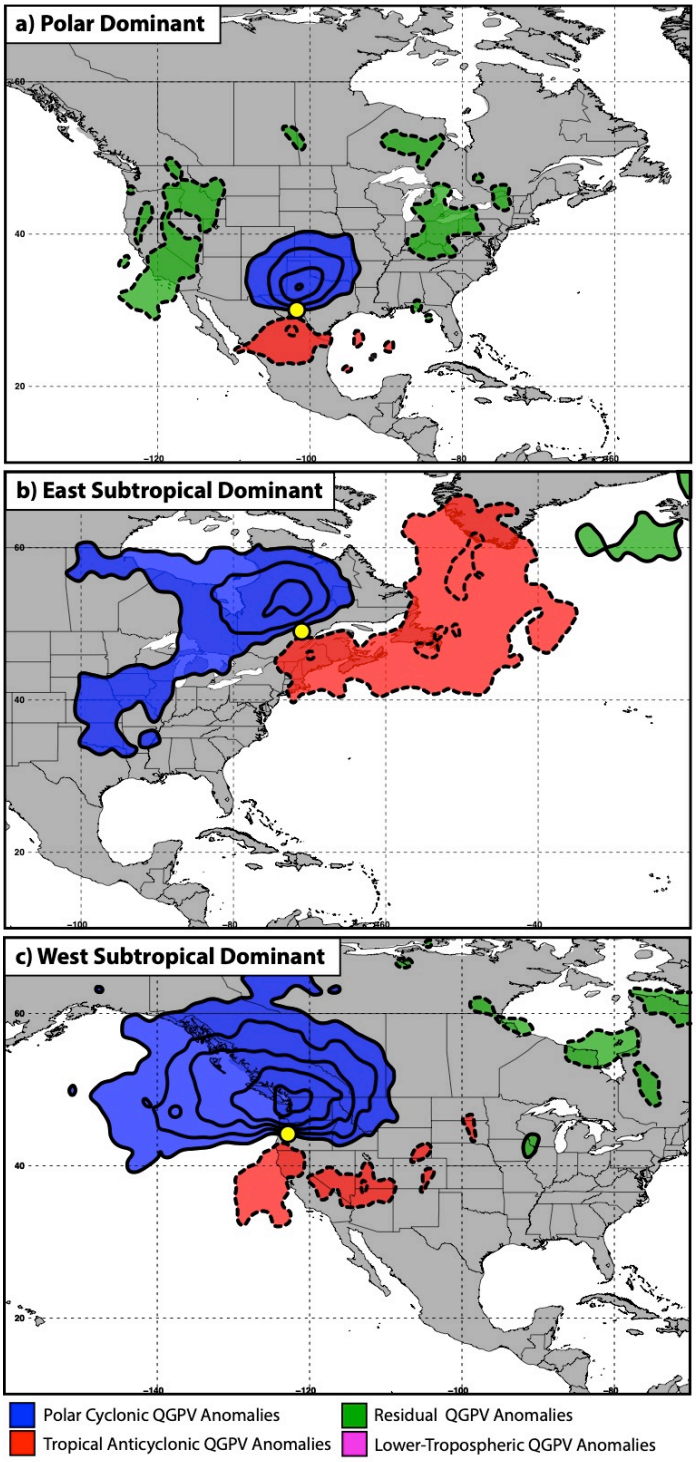

FIG. 5. 250-hPa QGPV anomalies (black lines every 4×10^{-5} s^{-1}, solid when positive and dashed when negative) at the time of superposition for polar dominant jet superposition events. The plotted QGPV anomalies are shaded to illustrate the QGPV classification scheme outlined in Table 1 and described in the text. (b) As in (a), but for 300-hPa QGPV anomalies at the time of superposition for eastern subtropical dominant events. (c) As in (a), but for 300-hPa QGPV anomalies at the time of superposition for western subtropical dominant events.

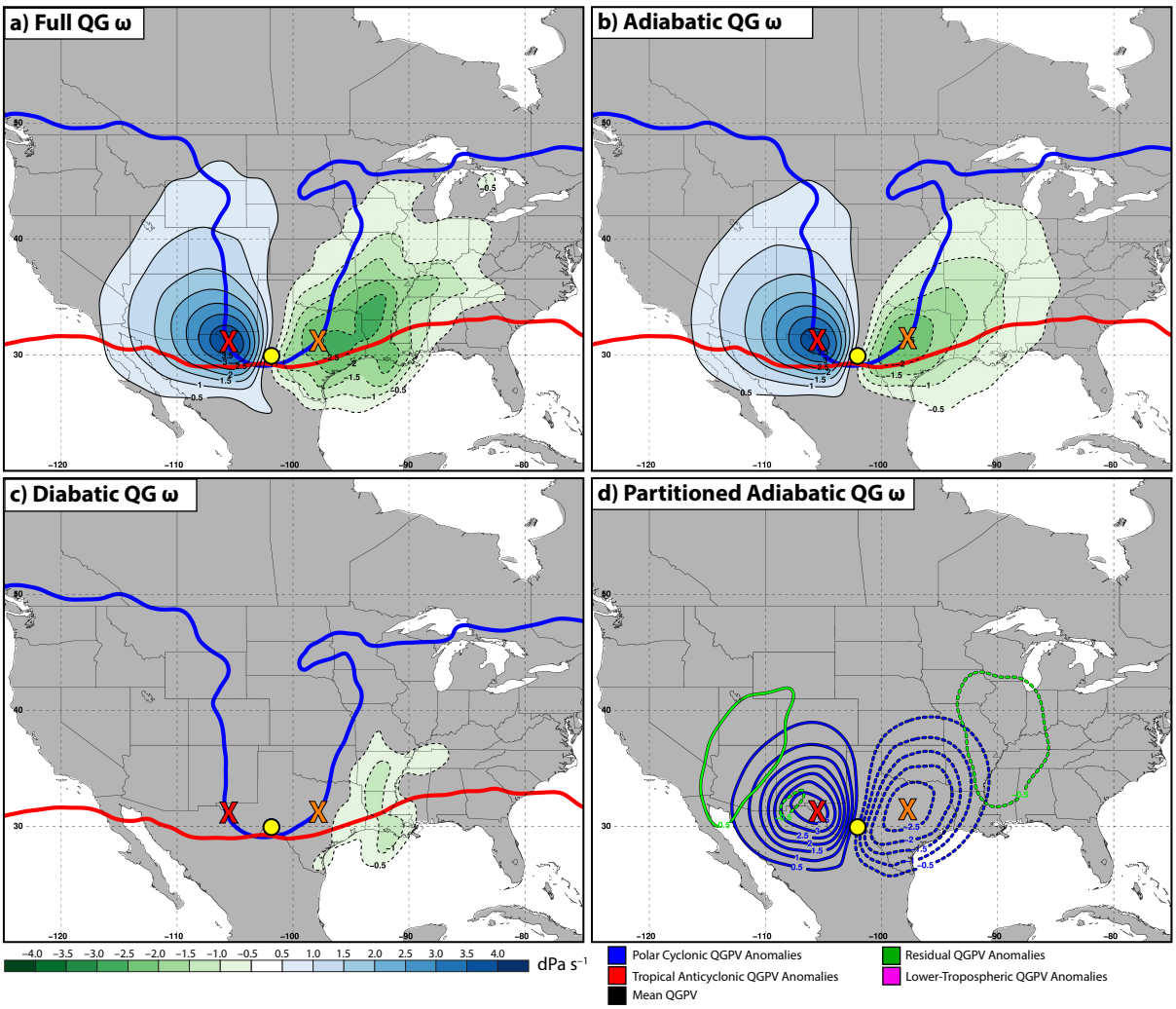

FIG. 6. (a) 500-hPa QG ω is shaded according to the legend in dPa s^{-1}, and the positions of the 2-PVU contour within the 320–325-K layer and 345–350-K layer at the time of a polar dominant jet superposition are indicated by the thick blue line and thick red line, respectively. (b) As in (a), but for the adiabatic contribution to the full QG vertical motion (ω_a). (c) As in (a), but for the diabatic contribution to the full QG vertical motion (ω_d). (d) The QG ω associated with each category of QGPV. Lines are plotted every 0.5 dPa s^{-1}, are solid when positive and dashed when negative, and are colored according to the categories of QGPV listed in the legend. In all panels, the yellow dot indicates the average location of jet superposition, and the red 'X' and orange 'X' denote the locations of maximum ω_a descent and ω_a ascent, respectively.

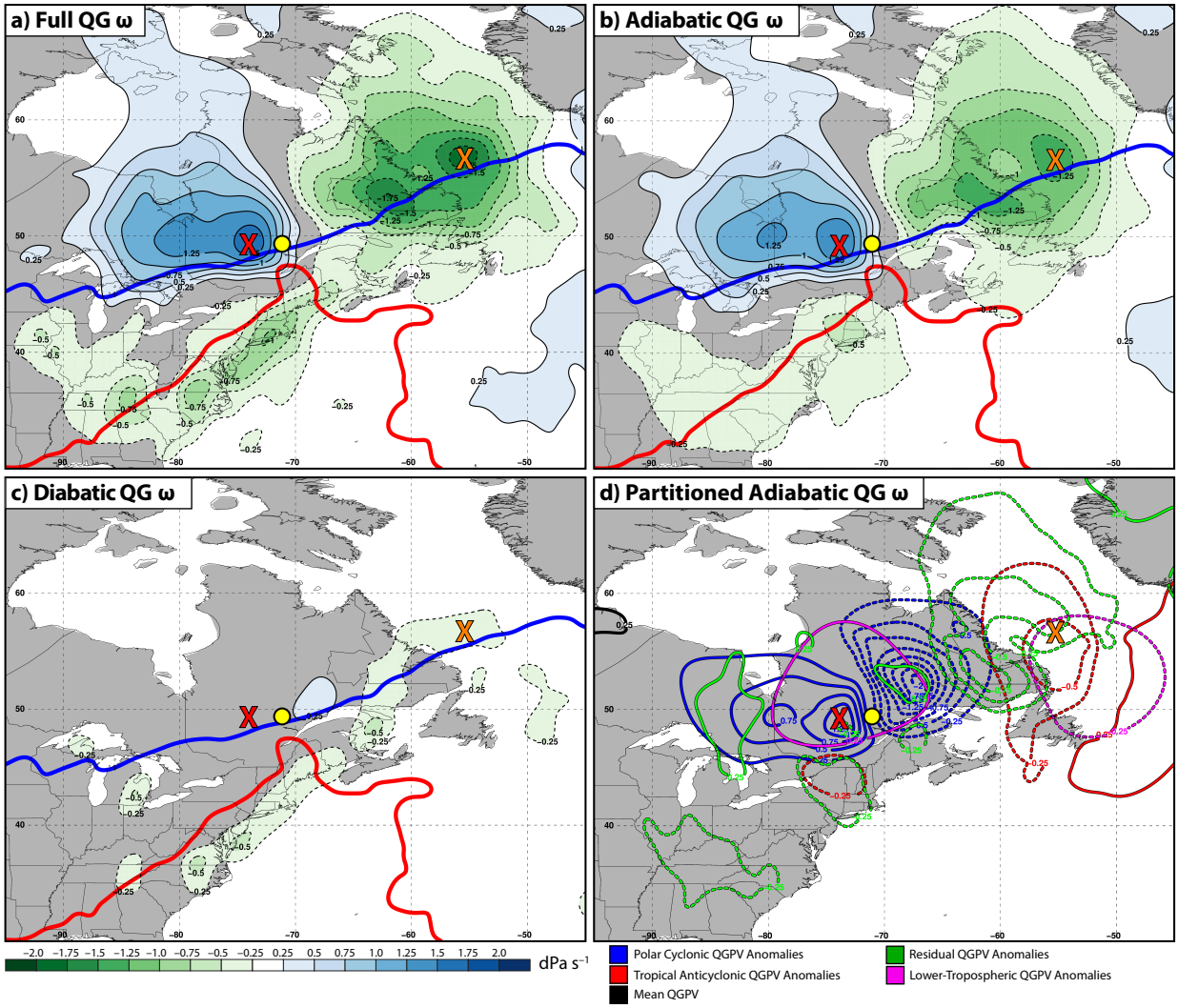

FIG. 7. As in Fig. 6, but at the time of an eastern subtropical dominant jet superposition. QG ω is shaded and contoured every 0.25 dPa s^{-1}.

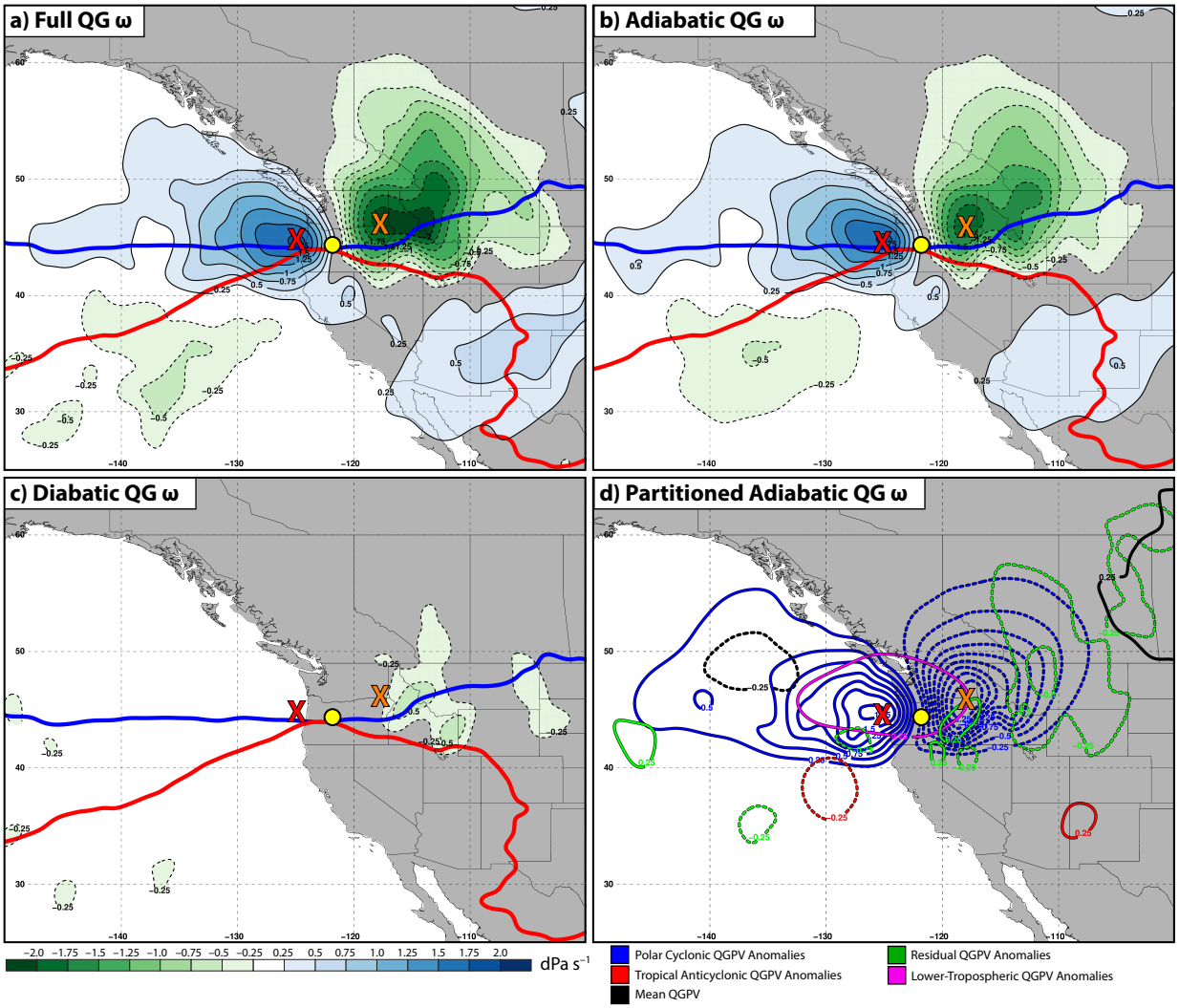

65 **FIG. 8**. As in Fig. 7, but at the time of a western subtropical dominant jet superposition.

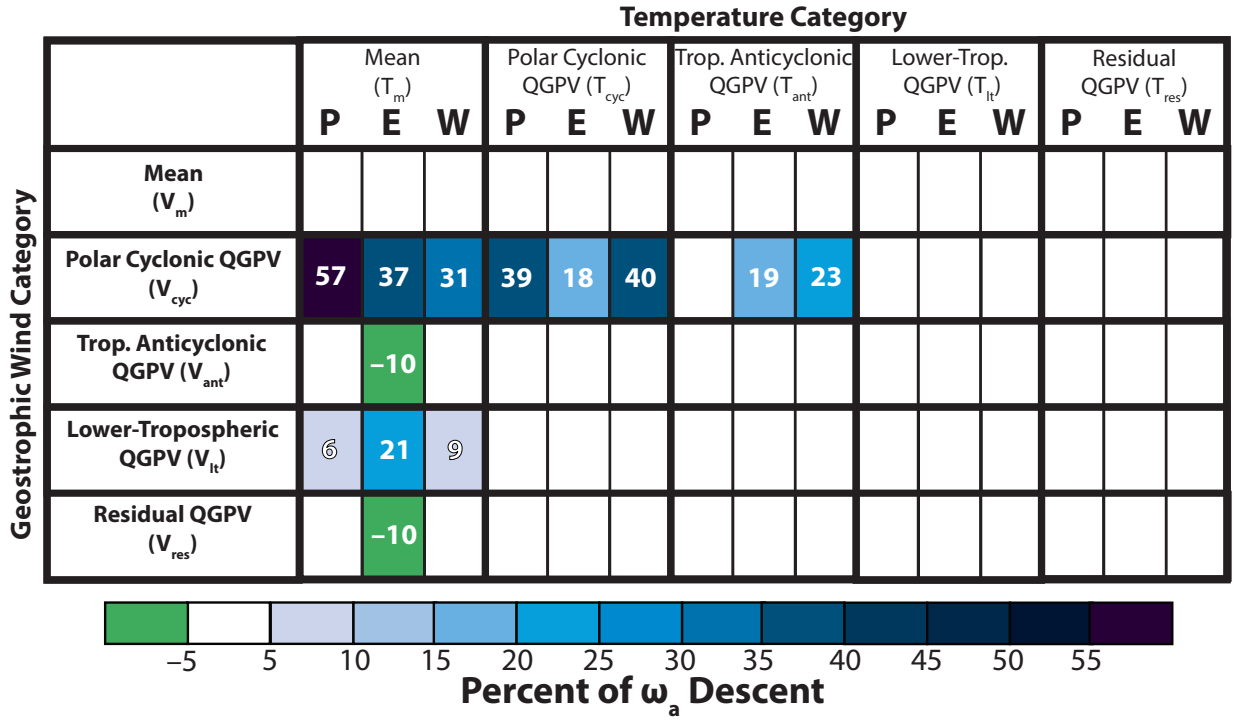

FIG. 9. The percent of the total ω_a descent (shaded according to the legend) that is associated with interactions between the geostrophic winds induced by each category of QGPV anomalies (rows), and the temperature fields associated with each category of QGPV anomalies (columns). The intersection of a row and column represents a particular interaction term, with the three boxes within an interaction term indicating the percent of ω_a descent that is associated with that interaction term at the location of maximum ω_a descent (red 'X's in Figs. 6–8) during polar dominant (P), eastern subtropical dominant (E), and western subtropical dominant (W) jet superposition events. The numeric percentage of ω_a descent associated with each interaction term is listed for those boxes in which the absolute value of the percent of ω_a descent is greater than 5%. Negative percentages correspond to interaction terms that are associated with QG ascent at the location of maximum ω_a descent.

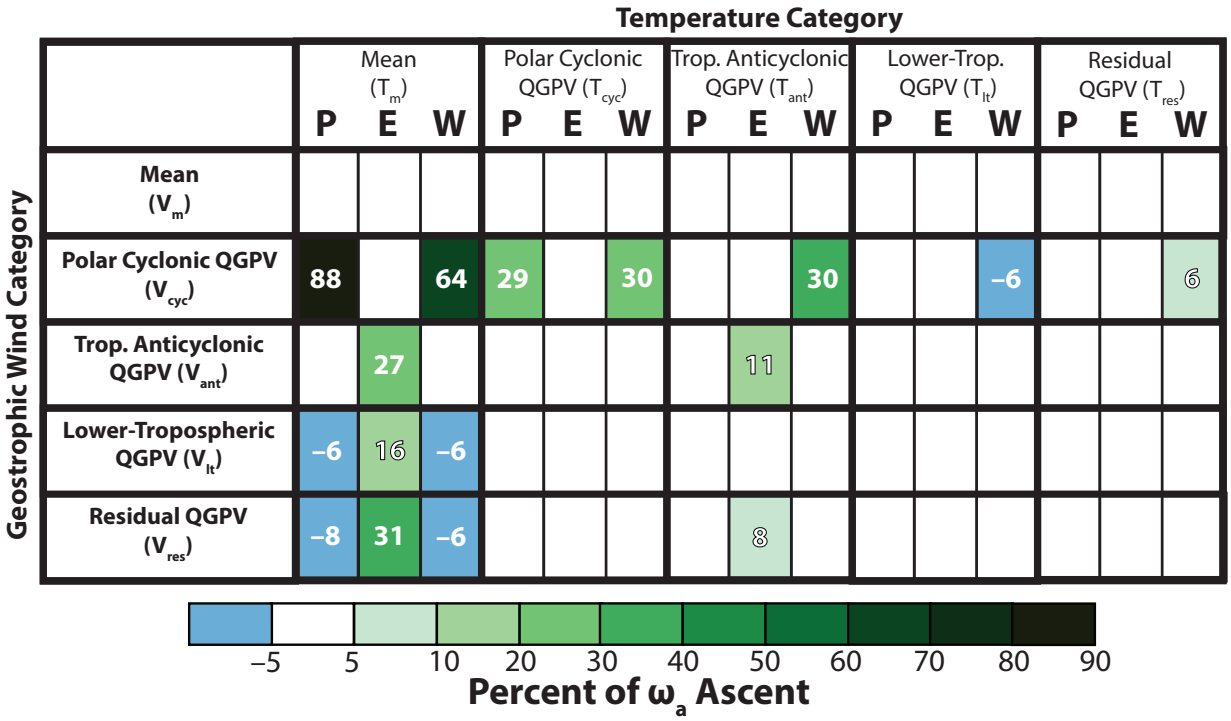

FIG. 10. As in Fig. 9, but for the percent of ω_a ascent (shaded according to the legend) that is associated with interactions between the geostrophic winds induced by each category of QGPV anomalies and the temperature fields associated with each category of QGPV anomalies at the location of maximum ω_a ascent (orange 'X's in Figs. 6–8) during polar dominant (P), eastern subtropical dominant (E), and western subtropical dominant (W) jet superposition events. The numeric percentage of ω_a ascent associated with each interaction term is listed for those boxes in which the absolute value of the percent of ω_a ascent is greater than 5%. Negative percentages correspond to interaction terms that are associated with QG descent at the location of maximum ω_a ascent.

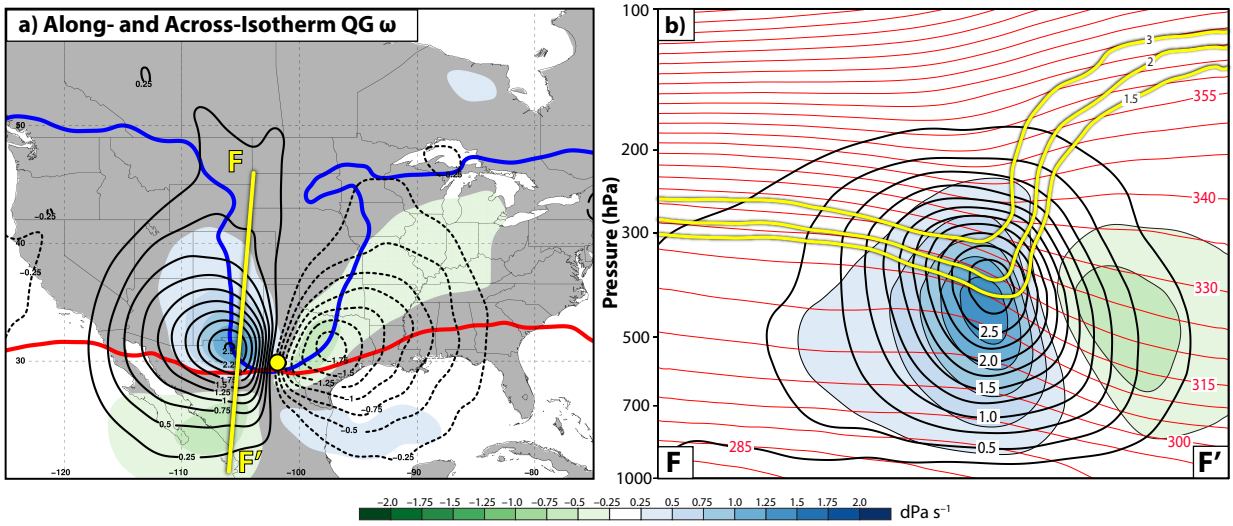

FIG. 11. (a) 500-hPa ω_n is shaded according to the legend in dPa s^{-1}, 500-hPa ω_s is contoured in black every 0.25 dPa s^{-1}, solid when positive and dashed when negative, and the positions of the 2-PVU contour within the 320–325-K layer and 345–350-K layer at the time of a polar dominant jet superposition are indicated by the thick blue line and thick red line, respectively. The yellow dot indicates the average location of jet superposition. (b) Cross section along F–F', as indicated in (a), with potential temperature (red lines every 5 K), the 1.5-, 2-, and 3-PVU contours (thick yellow lines), ω_n (shaded according to the legend in dPa s^{-1}), and ω_s (black contours every 0.25 dPa s^{-1} above 0.25 dPa s^{-1}).

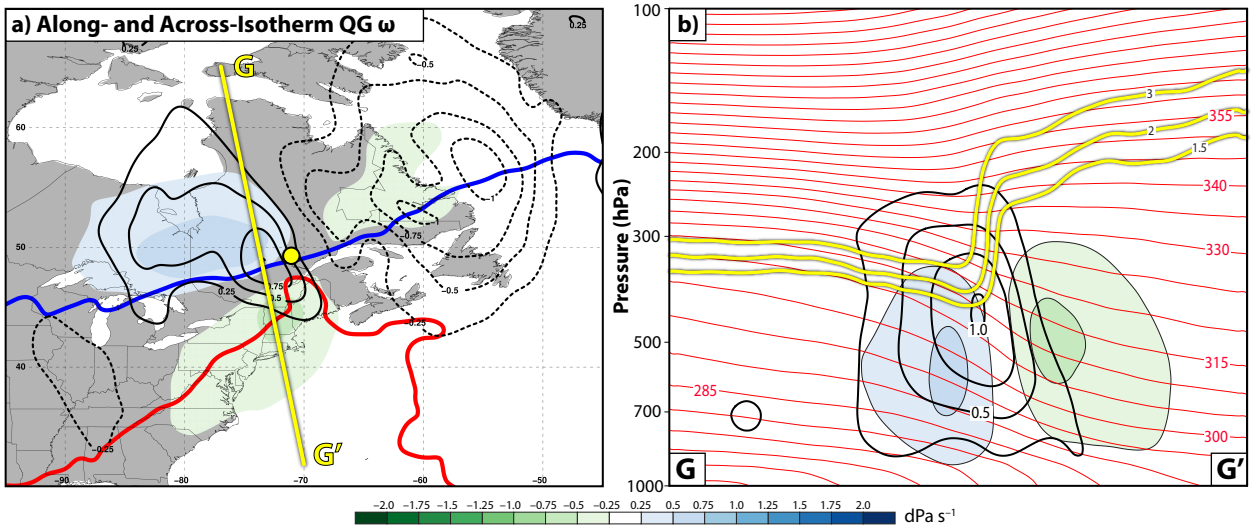

FIG. 12. (a) As in Fig. 11a, but for an eastern subtropical dominant jet superposition. (b) As in Fig. 11b, but for the cross section along G–G', as indicated in (a).

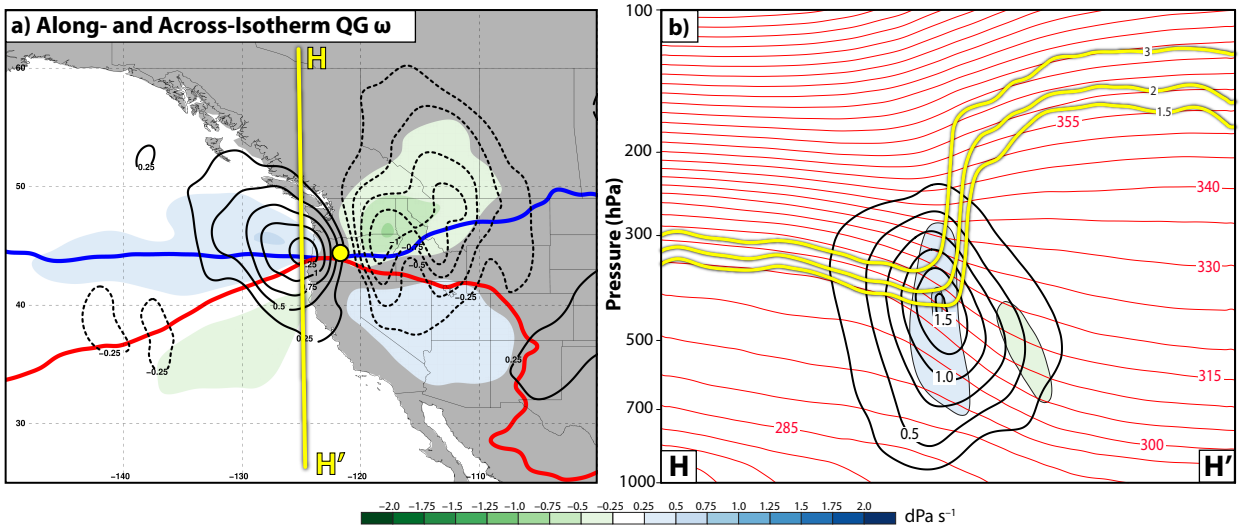

105
106 **FIG. 13**. (a) As in Fig. 11a, but for a western subtropical dominant jet superposition. (b) As in
107 Fig. 11b, but for the cross section along H–H', as indicated in (a).
108

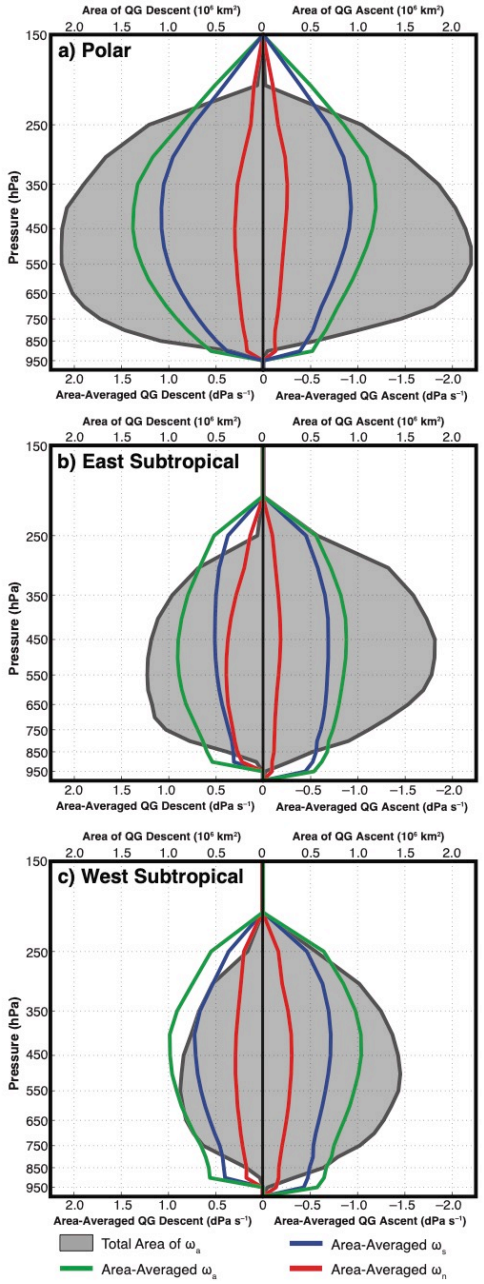

FIG. 14. (a) The area-averaged ω_a ascent downstream of polar dominant jet superpositions at locations in which $\omega_a < -0.5$ dPa s^{-1} (e.g., green shading in Fig. 6b) is shown as a function of pressure in green on the right-hand side of the plot. The area-averaged ω_a descent upstream of polar dominant jet superpositions at locations in which $\omega_a > 0.5$ dPa s^{-1} (e.g., blue shading in Fig. 6b) is shown in green on the left-hand side of the plot. The components of the area-averaged ω_a ascent and descent that can be attributed to ω_s and ω_n are indicated by the blue and red contours, respectively. The gray shading highlights the total area (in 10^6 km^2) of ω_a ascent or descent on each isobaric level that was used to calculate the area-averaged ω_a (e.g., the total area of green or blue shading at 500 hPa in Fig. 6b). (b) As in (a), but for eastern subtropical dominant jet superpositions. (c) As in (a), but for western subtropical dominant jet superpositions.